Geoderma 307 (2017) 54–64

Contents lists available at ScienceDirect

Geoderma

journal homepage: www.elsevier.com/locate/geoderma

Role of biological soil crusts in affecting soil evolution and salt geochemistry in hyper-arid Atacama Desert, Chile

Fan Wang[a,b,*], Greg Michalski[b,c], Hao Luo[c], Marc Caffee[b,d]

[a] School of Environment and Energy, Peking University Shenzhen Graduate School, Shenzhen, Guangdong Province 518055, China
[b] Department of Earth, Atmospheric and Planetary Sciences, Purdue University, West Lafayette, IN 47907, USA
[c] Department of Chemistry, Purdue University, West Lafayette, IN 47907, USA
[d] Department of Physics and Astronomy, Purdue University, West Lafayette, IN 47907, USA

ARTICLE INFO

Handling Editor: M. Vepraskas

Keywords:
Biological soil crusts
Atacama Desert
Nitrate oxygen isotope
Chlorine 36
Soil accumulation mechanism

ABSTRACT

Eight soil profiles, either barren or covered with biological soil crusts (BSCs), were sampled at multiple depths in a remote valley in the Atacama Desert, Chile, to explore the impact of BSCs on soil evolution and salt geochemistry. BSC sites had thicker soil profiles compared to non-BSC sites, which could be a result of past geological processes and also partially accounted for by the establishment of BSCs that can help limit erosion and promote significant soil accumulation. The greater abundances of fine particles below BSCs could essentially be attributed to the ability of BSCs to trap more fine grains. The generally higher salt ion inventories but smaller salt ion concentrations in soil profiles beneath BSCs were probably due to that BSCs can promote the retention of salt ions and insoluble dust simultaneously, but the latter to a greater extent. Nitrate oxygen isotopes indicated the predominant existence of atmospheric nitrate in the soils, suggesting biological processes of BSCs may not significantly impact the ion accumulation or distribution in the underlying soils. A mechanism of consistent soil accumulation via the retention of atmospheric deposition and occasional interruption of subsurface collapsing due to erosion processes was proposed to explain the development of soil profiles and different landscape features as well as the role of BSCs in soil evolution in this study area. The soil ages were estimated to be around 440 ky based on the proposed soil accumulation mechanism.

1. Introduction

The Atacama Desert in northern Chile is one of the driest places on Earth, where hyper-arid climate precludes establishment of vegetation across much of the desert, resulting in a vast barren land susceptible to wind erosion (Ericksen, 1981; McKay et al., 2003). Wind erosion is significant in most parts of the Atacama as evidenced by high winds, high eolian particle loads and widespread wind erosional features (Stoertz and Ericksen, 1974; Flores-Aqueveque et al., 2012). In comparison, water erosion is relatively minor in the Atacama, only occurring during rare rainfall events or in certain regions with ephemeral rivers or groundwater systems (Placzek et al., 2010). Wind erosion can be offset by the deposition of dust (insoluble particles) and salts from the atmosphere (Michalski et al., 2004; Ewing et al., 2006; Wang et al., 2015), with the net balance between deposition and erosion being a function of the surface stability. Given the lack of vegetation in the Atacama, the surface stability is mainly modulated by surface geomorphology. Desert pavement is a ubiquitous geomorphic feature in arid environments, including the Atacama, characterized by a layer of loosely cemented, interlocking clasts that can protect the surface from erosion (Cooke, 1970) and lead to an inflationary surface (McFadden et al., 1987). Low solubility gypsum/anhydrite crusts often form beneath desert pavements in the Atacama via gypsum dissolution and rapid recrystallization, which further armors the underlying soil profiles from erosion (Ericksen, 1981). The balance between deposition and erosion at one of the Atacama's driest locations, with a sparse desert pavement and 15 cm deep gypsum blocks, indicated that these protection mechanisms only resulted in the retention of about 20% of the deposited dust (Wang et al., 2015), reflecting the generally weak surface stability and very slow soil accumulation rates in the Atacama.

Biological soil crusts (BSCs) are another kind of soil surface cover common in deserts. BSCs can significantly influence soil stability and nutrient cycling (Belnap, 2003, 2006). BSCs are living consortia of cyanobacteria, green algae, lichens, and mosses that can survive in extremes of cold, heat, and aridity (Belnap, 2003). BSCs can reduce wind erosion in deserts (Leys and Eldridge, 1998; Belnap et al., 2014) probably because of exuding extracellular polysaccharides that bind soil particles together (Belnap and Gardner, 1993). Further, BSCs

* Corresponding author at: School of Environment and Energy, Peking University Shenzhen Graduate School, Shenzhen, Guangdong Province 518055, China.
E-mail address: wangfan@pkusz.edu.cn (F. Wang).

http://dx.doi.org/10.1016/j.geoderma.2017.07.035
Received 5 October 2016; Received in revised form 19 July 2017; Accepted 26 July 2017

potentially modify soil surface roughness, porosity, and aggregations to reduce water erosion by increasing infiltration and enhancing water retention (Belnap, 2006). More importantly, BSC communities are considered “unique” in that they are often key photoautotrophic microorganisms and primary producers in extreme environments (Büdel, 2001). They can become biologically active by absorbing brief pulses of water (Belnap et al., 2004), resulting in high instantaneous rates of carbon and nitrogen fixation (Evans and Lange, 2001; Belnap, 2002; Housman et al., 2006) as well as the ability to exude nitrate into soil (Gaio-Oliveira et al., 2005; Johnson et al., 2007). Therefore, BSCs contribute significantly to desert ecosystem fertility and aid in the evolution and spread of other terrestrial life forms.

Despite significant advances in our understandings of the role of BSCs in affecting soil evolution and geochemical cycling, there are still unanswered questions. For example, the rate of soil stabilization caused by BSCs has yet to be quantified and their role in altering soil grain size distribution is still not completely understood (Li et al., 2005; Belnap, 2006; Zhao et al., 2010). The amount of soil nitrate produced by BSCs versus deposited from the atmosphere, which is significant in deserts (Michalski et al., 2004; Wang et al., 2016), is another open question. On the whole, the detailed impact mechanism of BSCs on soil evolution and geochemical cycles in desert ecosystems is not sufficiently studied, especially in hyper-arid regions. Therefore, this study was conducted in the Atacama Desert to compare soil profiles with and without BSCs using physiochemical and isotopic techniques, aiming to constrain the role of BSCs in affecting soil evolution and salt geochemistry in hyper-arid regions.

2. Study area

Widespread BSC communities were identified in a remote valley (~21.22°S, 69.90°W, ~800 m a.s.l.) in the Atacama's Coastal Range during field work in December of 2011 at the southeastern edge of the Salar Grande, a basin filled with massive salt mineral deposits (Stoertz and Ericksen, 1974) (Fig. 1). Halite (NaCl) is the principal mineral of the Salar Grande evaporites and is the underlying strata on which soils developed (Stoertz and Ericksen, 1974). Despite the modern mean annual precipitation (MAP) < 2 mm as recorded at the Iquique (100 km northwest) and Quillagua (60 km southeast) rain gauge stations (Houston, 2006), there are likely repeated occurrences of fog (~20 days per year) in the valley (Fig. 2A) based on its geographic similarities to some other foggy sites along the coastal Atacama (Cereceda and Schemenauer, 1991) and field observations. Because of the steep Coastal Range, fog condensation is concentrated in a narrow belt extending the elevation from 300 to 800 m (Rundel, 1978) that sufficiently supports the vegetation evolution (Fig. 2B). The Salar Grande region has been reported to have abundant lichen epiphytes (association of cyanobacteria, algae and fungi) (Conley et al., 2006; Follmann, 2008), and the association of cyanobacteria and bacteria were even found on the near surface of salt nodules (Stivaletta et al., 2012).

The landscape along the southeastern rim of the Salar Grande contains three major features: barren ground, BSC-covered ground and depression pits, with transitions between these three features occurring over a narrow distance (10–100s of meters) (Fig. 2). On the barren ground, there are typically no visible BSC communities. The surface is sparsely covered with 0.5–1 cm reddish to tannish pebbles, with decimeter to meter-sized polygonal fracture patterns observed beneath (Fig. 2C). Marginal open fissures along the polygon edges, likely caused by desiccation or thermal expansion, are filled with salt-cemented sand, silt, and rock debris and have been termed “sand dikes” (Ericksen, 1981). The BSC-covered grounds have a hummock relief of ~50 cm and 80–90% of their surfaces are covered with BSCs. The BSC colonies are fractured into small brittle patches (Fig. 2D), typically 10 cm in diameter, probably because of differential drying between the upper and lower crust surfaces (Belnap, 2006). The hummocky BSC-covered

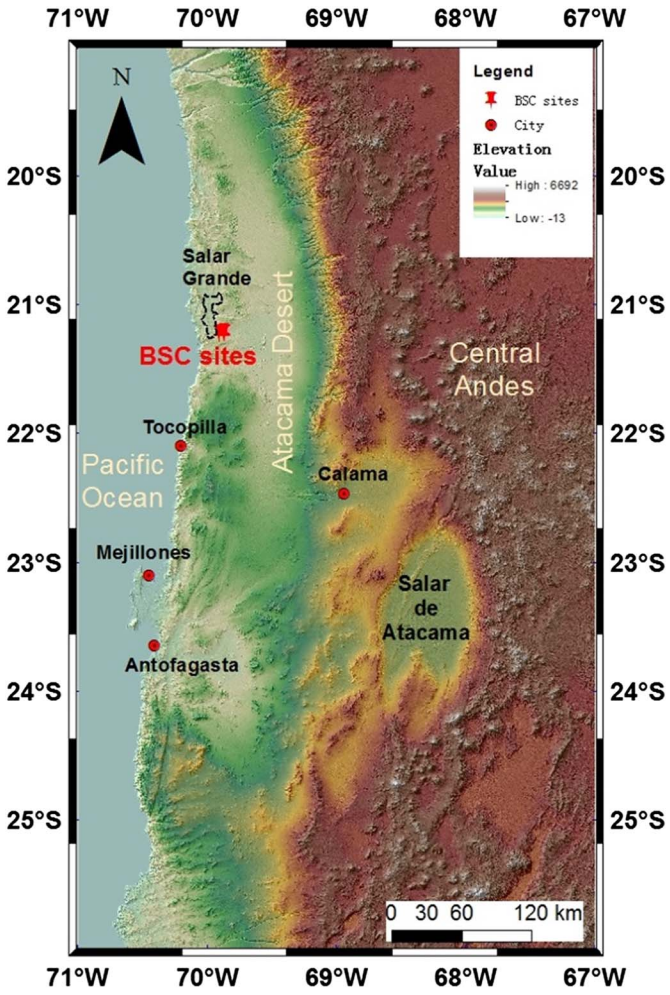

Fig. 1. Map of the Atacama Desert in northern Chile showing the location of the BSC soil sampling transects (red pin) near the edge of Salar Grande (outlined by black dash lines), just north of the city of Tocopillo (red dot). (For interpretation of the references to color in this figure legend, the reader is referred to the web version of this article.)

grounds are intervened by depression pits (~2–5 m in diameter) that are scattered across the surface and were likely formed by ephemeral streams causing subsurface salt dissolution and surface collapse (Stoertz and Ericksen, 1974). There are no BSCs but widespread white salt nodules, mainly halite, in the depression pits (Fig. 2E), which probably formed from hard, dense and crystalline halite by slow solution and recrystallization due to frequent wetting with coastal fogs (Stoertz and Ericksen, 1974). These salt nodules (Site 8) suggest that strong capillary rise of concentrated brines occurred in the past, and this extreme salinization was probably harmful and thus prevented the BSC establishment in the depression pit (Amit et al., 2010).

3. Sampling and analysis methods

Eight soil pits were dug along two approximately north-south transects that are ~4 km apart; Transect 1 spanned over 1000 m from the north side to the south side of a hummocky ground, while Transect 2 was only 70 m long and located on the south side of another hummocky ground (Fig. 2F). Sites 2, 3, 5 and 6 were BSC sites with BSC coverage all located on the BSC-covered grounds, but Sites 3 and 6 were in the transition zones (the edge of the depression pit and the edge of BSC-covered ground, respectively) with slightly less BSC coverage (Fig. 2F). Sites 1, 4, 7 and 8 were non-BSC sites with no BSC coverage; Sites 1, 4 and 7 were located on the barren grounds while Site 8 was located in a depression pit on the BSC-covered ground (Fig. 2F). Each

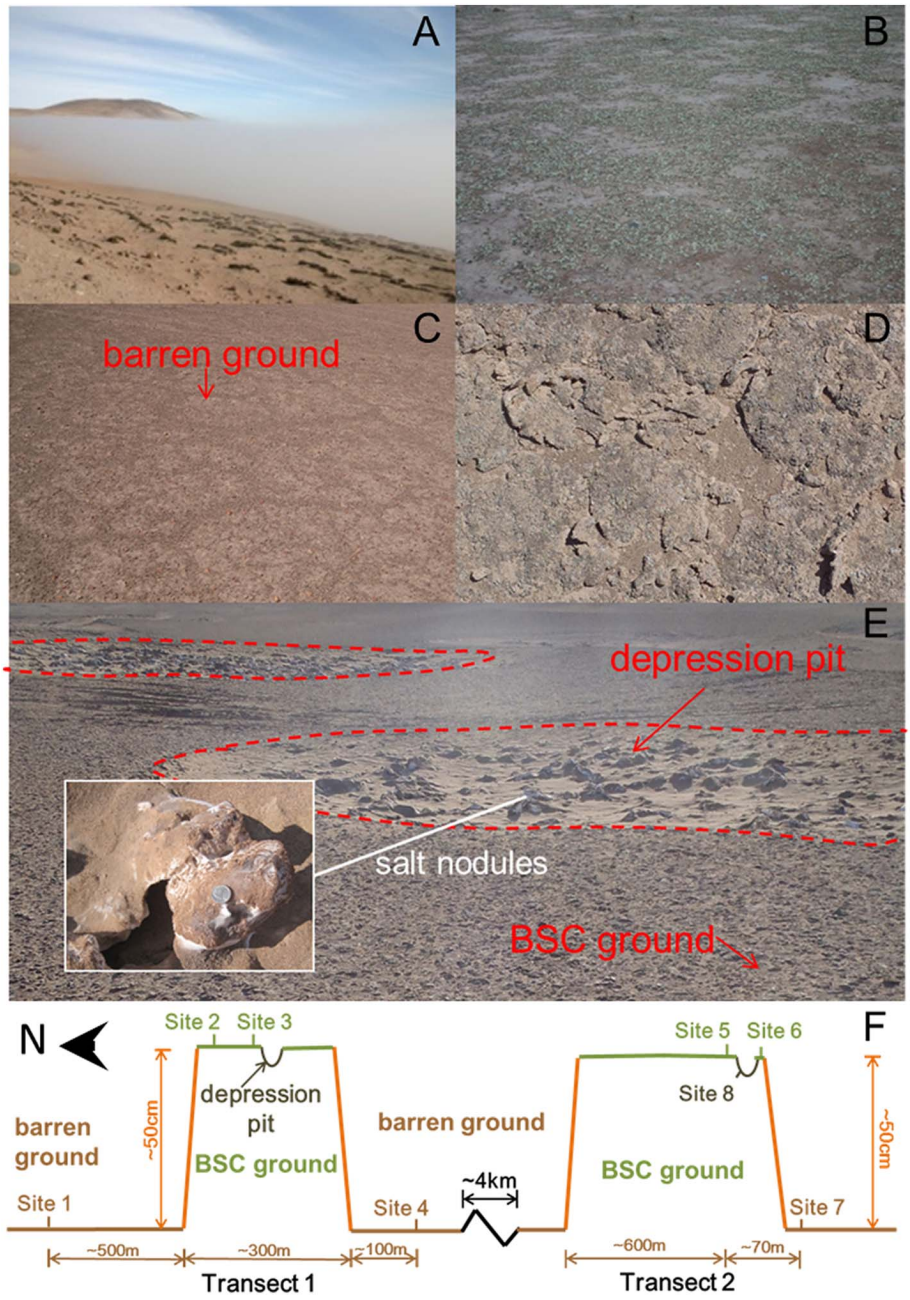

Fig. 2. An example of a fog incursion from the Pacific Ocean coast into Salar Grande (A) that can supply water to biological soil crusts that blanket the lower parts of the valley (B). There are abrupt transitions from polygon-type barren surfaces (C) or depression pits (E) to the fractured and upturned crust surfaces (D). This transition occurs over a narrow distance (10–100s of meters). The depression pits are lined with white salt halite nodules. A diagram shows the distribution of sampling sites along two transects (not to scale) (F).

Table 1
Detailed site descriptions and sampling depths.

Sampling site	Geological unit	BSC coverage	Sampling depth
Transect 1			
Site 1	Barren ground	No	15 cm
Site 2	BSC-covered ground	Yes	70 cm
Site 3	The edge of the depression pit	Yes	40 cm
Site 4	Barren ground	No	20 cm
Transect 2			
Site 5	BSC-covered ground	Yes	60 cm
Site 6	The edge of BSC-covered ground	Yes	25 cm
Site 7	Barren ground	No	15 cm
Site 8	Depression pit	No	20 cm

soil pit was excavated to the depth where a hard salt layer, likely the salar bed, was reached (Table 1). Samples were obtained from discrete depths in each soil pit, and the surface samples of Sites 2, 3 and 5, are biological soil crust samples.

Microscope images were taken of the BSCs, and the soils were analyzed for grain size, water soluble ions, the cosmic-ray radioactive nuclide ^{36}Cl and stable oxygen isotopes of nitrate (^{17}O and ^{18}O). BSCs were observed under an Olympus BX51 polarized light microscope (Olympus America, Center Valley, PA, USA) equipped with a digital camera. The bulk soil density was measured using a graduated measuring cylinder with 10 g slightly compacted soil. Large aggregates of soil were gently broken up and a dry sieve analysis was conducted to study the grain size distribution as a function of depth. A split of each soil sample was homogenized and ground by a ball mill or hand. Soluble salts were extracted with Milli-Q Millipore™ water (ultrapure 16 MΩ·cm) in a roughly 1:10 mass ratio (soil to water). A series of

geochemical and isotopic analysis was subsequently performed on the soil extracts. Cation (Ca^{2+}, Na^{+}, Mg^{2+} and K^{+}) concentrations were determined using Thermo Scientific iCAP 6500 inductively coupled plasma-optical emission spectroscopy (ICP-OES) (Thermo Scientific, Pittsburgh, PA, USA), while anions (Cl^{-}, NO_3^{-} and SO_4^{2-}) were analyzed using Dionex DX-500 ion chromatography system (Dionex Corp., Sunnyvale, CA, USA). Ion inventories for a given excavation pit were calculated by integrating the ion masses (multiplying the ion concentrations with soil density) over the entire sampling depths. A soil extract split was analyzed for $\delta^{17}O$ and $\delta^{18}O$ values of nitrate using a recent bacterial reduction, gold redox method (Kaiser et al., 2007; Riha, 2013). The δ term is the isotope ratio relative to an accepted standard (in units of per mil): $\delta‰ = [(R_{sample} / R_{standard}) - 1] \times 10^3$, where R is the ratio of the minor to major isotopes (i.e. $^{18}O/^{16}O$ or $^{17}O/^{16}O$); Vienna standard mean ocean water (VSMOW) ($^{18}O/^{16}O = 2005.20 \pm 0.43$ ppm, $^{17}O/^{16}O = 379.9 \pm 1.6$ ppm) (Craig, 1961) is the adopted international oxygen isotope standard. Another split of the soil extract was used to analyze the ^{36}Cl isotope composition (301 ky half-life) by first completely removing SO_4^{2-} using excess $Ba(NO_3)_2$, and precipitating $AgCl_{(s)}$ using $AgNO_3$ in excess (Hainsworth et al., 1994). $AgCl_{(s)}$ was isolated by centrifugation and filtration, washed 5 times with Milli-Q Millipore™ water, and freeze-dried. The purified $AgCl_{(s)}$ was loaded into a copper target and analyzed for the $^{36}Cl/Cl$ (i.e. $^{35}Cl + {}^{37}Cl$) ratio by accelerator mass spectrometry (AMS) at the Purdue Rare Isotope Measurement (PRIME) laboratory according to the general methodology by Sharma et al. (2000). ^{36}Cl inventories were calculated by integrating the ^{36}Cl amount (multiplying ^{36}Cl concentrations and soil density) over the entire sampling depths.

Statistical analysis, i.e. General Linear Model-Multivariate Analysis of Variance (GLM-MANOVA), was performed by the statistical software package PASW Statistics 18.0 (SPSS Inc., Chicago, IL, USA) to investigate the impact of BSCs on the grain size and ion distribution. The existence of BSC coverage (i.e. with BSCs and without BSCs) was selected as the fixed factor, and the percentages of five grain size fractions or different ion concentrations/inventories as the dependents. The $p < 0.05$ was considered statistically significant, and $p < 0.01$ was considered highly significant. Samples from different depths were not differentiated during the GLM-MANOVA analysis.

4. Results

4.1. Crust morphology

The morphology of BSC colonies attached to a sand grain (approximately 1 mm in diameter) observed under the microscope was typically that of white cerebrum-shaped clusters (Fig. 3). The surfaces of most BSC colonies were dotted with linear bead structures, while some BSC clusters were deep brown to black (Fig. 3). Clear-white filament-like structures were also observed.

4.2. Soil profile depth and size distribution

The loose soil profiles above the hard salt layer were all thicker beneath BSCs than at non-BSC sites (Table 1). The loosely-cemented powdery soil extended to depths of 70 cm and 60 cm beneath BSCs at Sites 2 and 5, respectively, but reached only 15–20 cm depth beneath the barren ground (Sites 1, 4 and 7) and in the depression pit (Site 8). Two soil profiles located in the transition zones (Sites 3 and 6) had loose soil profiles ranging from 25 to 40 cm deep.

The bulk density of loose soil was relatively consistent of ~1.4 g cm^{-3} at different depths from different profiles, while the soil particle composition showed variations between depths among different sites. The soil particles consisted of mostly sand (63–2000 μm diameter) and only 1–39% silt and clay (< 63 μm) according to the grain size classification method specified by Krumbein and Sloss (1963). The largest percentages for the two finest grain size fractions (63–125 μm and < 63 μm) both occurred at BSC sites (Fig. 4); the GLM-MANOVA analysis confirmed that the 63–125 μm and < 63 μm fractions differed between in BSC soils (more fine grains) and in non-BSC soils (less fine grains) ($p < 0.05$). The finest grain-sized samples in the barren ground soil profiles were on the surface, while the BSC-covered grounds or transition sites had the finest grain-sized samples at depths around 10–15 cm (Fig. 4).

4.3. Soil ion distribution and isotopic composition

Generally, for all the sites, soil Na^{+}, K^{+}, Mg^{2+}, Cl^{-} and NO_3^{-} concentrations were almost nil on the surface, while Ca^{2+} and SO_4^{2-} were widespread throughout the soil profiles. The Ca^{2+}/SO_4^{2-} molar ratios were 0.75–1.09 in the upper 10 cm of the soil profiles, but SO_4^{2-} was in large excess over Ca^{2+} at depths > 10 cm. The Ca^{2+} and SO_4^{2-} inventories were 52–202 mol m^{-2} and 74–413 mol m^{-2}, respectively. Beneath the surface, the soluble ions were dominated by Na^{+} and Cl^{-} with the inventories of 493–2038 mol m^{-2} and the Na^{+}/Cl^{-} molar ratios of approximately 1. There were also significant amounts of K^{+} (inventories: 4–86 mol m^{-2}), Mg^{2+} (21–258 mol m^{-2}), and NO_3^{-} (4–12 mol m^{-2}) beneath the surface.

The soil ion concentrations (mmol (g soil)$^{-1}$) were generally lower below BSCs than at non-BSC sites (Figs. 5 and 6). The GLM-MANOVA analysis revealed that there were significant systematic differences in the concentrations of most ions between BSC sites and non-BSC sites ($p < 0.05$ for Na^{+}, Cl^{-}, Mg^{2+}, and $p < 0.01$ for NO_3^{-}). Instead, all the ion inventories, except for NO_3^{-}, at BSC sites were 1.7–7.0 times of those on barren grounds (Site 2 versus Site 4, Sites 5 and 6 versus Site 7) ($p < 0.01$). The ion inventories were also relatively large in the depression pit (Site 8), while the ion inventories on the edge of the depression pit (Site 3) were low.

Soil nitrate $\Delta^{17}O$ values ($\Delta^{17}O = \delta^{17}O - 0.52 * \delta^{18}O$) ranged from 18.2–26.6‰ and generally decreased with depth with peak values occurring on the surface 0–1 cm. There is a positive correlation between $\Delta^{17}O$ and $\delta^{18}O$ (Fig. 7). The $^{36}Cl/Cl$ ratios ranged from

Fig. 3. Light microscope images of BSC colonies attached to sand grains (~1 mm in diameter). (For interpretation of the references to color in this figure, the reader is referred to the web version of this article.)

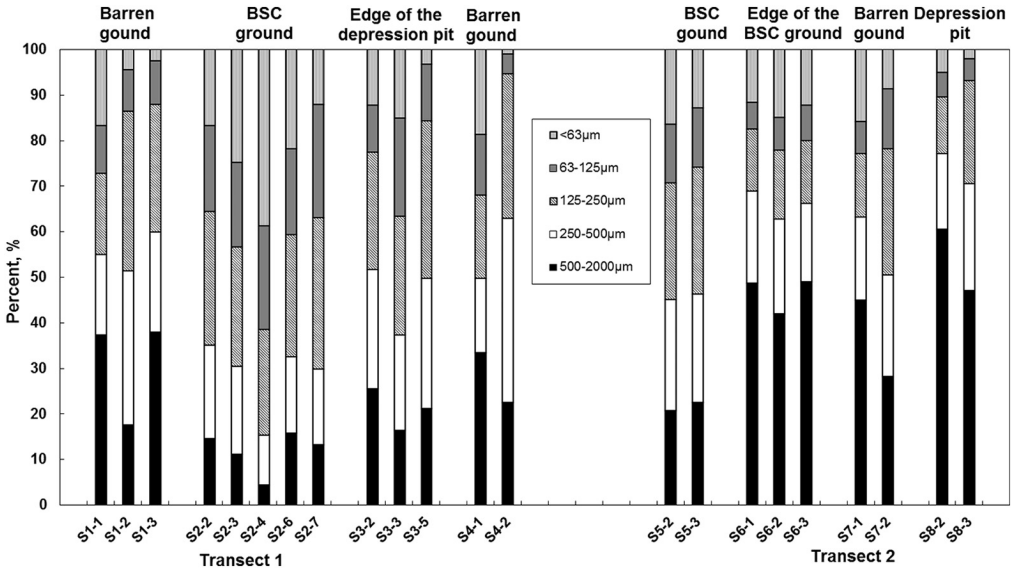

Fig. 4. The grain size distribution of soils collected at different depths across Transects 1 and 2. The X-axis labels indicate the sample IDs with the first number delineating the site number and the second number after the dash delineating the sample order at each sampling site. The surface samples at Sites 2, 3 and 5, i.e. S2-1, S3-1, and S5-1, are biological soil crust samples and thus not measured for grain size distributions.

37.4–398 $\times$ 10^{-15} with the largest $^{36}Cl/Cl$ ratio of 398 $\times$ 10^{-15} occurring on the surface clast at Site 1 located on the barren ground (Table 2). The surface crust and underlying soil (0–1 cm layer beneath the crust) at BSC Site 2 were not analyzed for ^{36}Cl analysis because of low Cl^- concentrations and the lack of sufficient amounts of chloride extracted from soil samples. The ^{36}Cl inventory of 1.2 $\times$ 10^{14} atoms m^{-2} at Site 2 on the BSC-covered ground was larger than that of 7.6 $\times$ 10^{13} atoms m^{-2} at Site 1.

5. Discussion

5.1. BSC type and components

These BSCs are likely dominated by the genus *Roccellina*, a crustose lichen described by Tehler (1983) and Follmann (2008). The linear beads on the surfaces and filament structures (Fig. 3) are probably fungal hyphae. The *Roccellina* genus includes 18 species that are endemic in Pacific South America, 16 of which are distributed across central to northern Chile (Follmann, 2008). These BSCs are visually similar to the lichen species *Roccellina cerebriformis* (Mont.) Tehler (Tehler, 1983) which has been previously reported to exist in the coastal mountain ranges near Iquique, 15 km southwest of our site

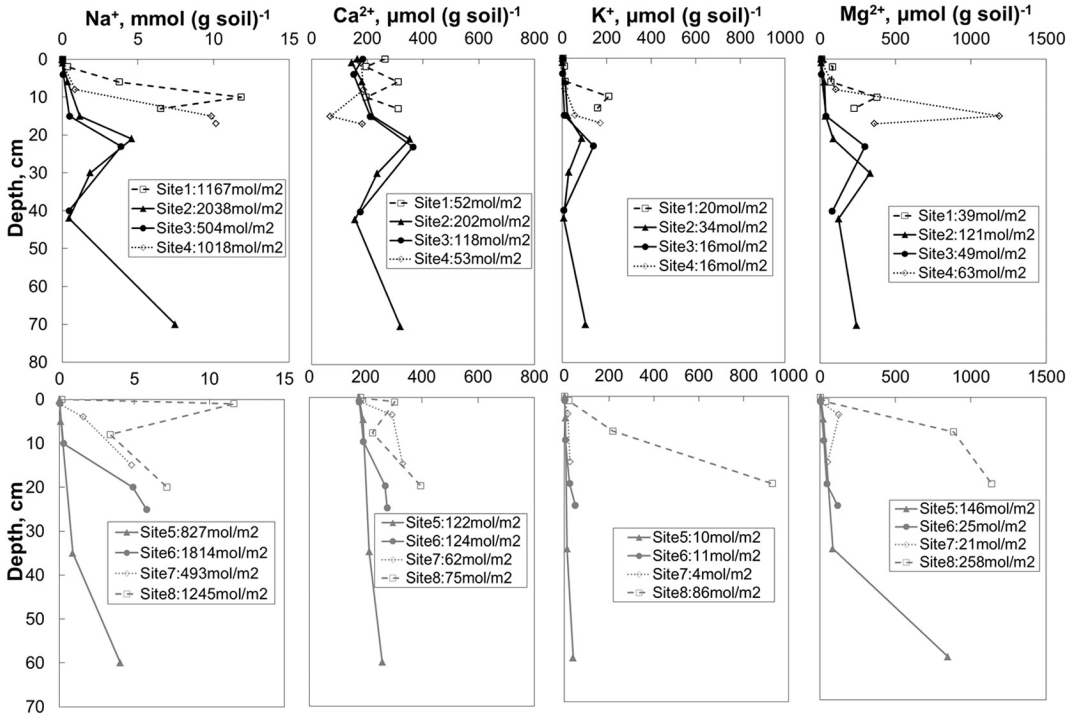

Fig. 5. The cation distribution as a function of depth for different sites along Transect 1 (upper panel) and Transect 2 (lower panel). Salt inventories are listed after the site number in the legend. Solid lines with solid-filled symbols in black or grey represent the BSC sites while dash lines with empty-filled symbols represent non-BSC sites. The surface samples at Sites 2, 3 and 5 are biological soil crust samples and their ion concentrations should be in the unit of mmol (g dry mass)$^{-1}$ or μmol (g dry mass)$^{-1}$.

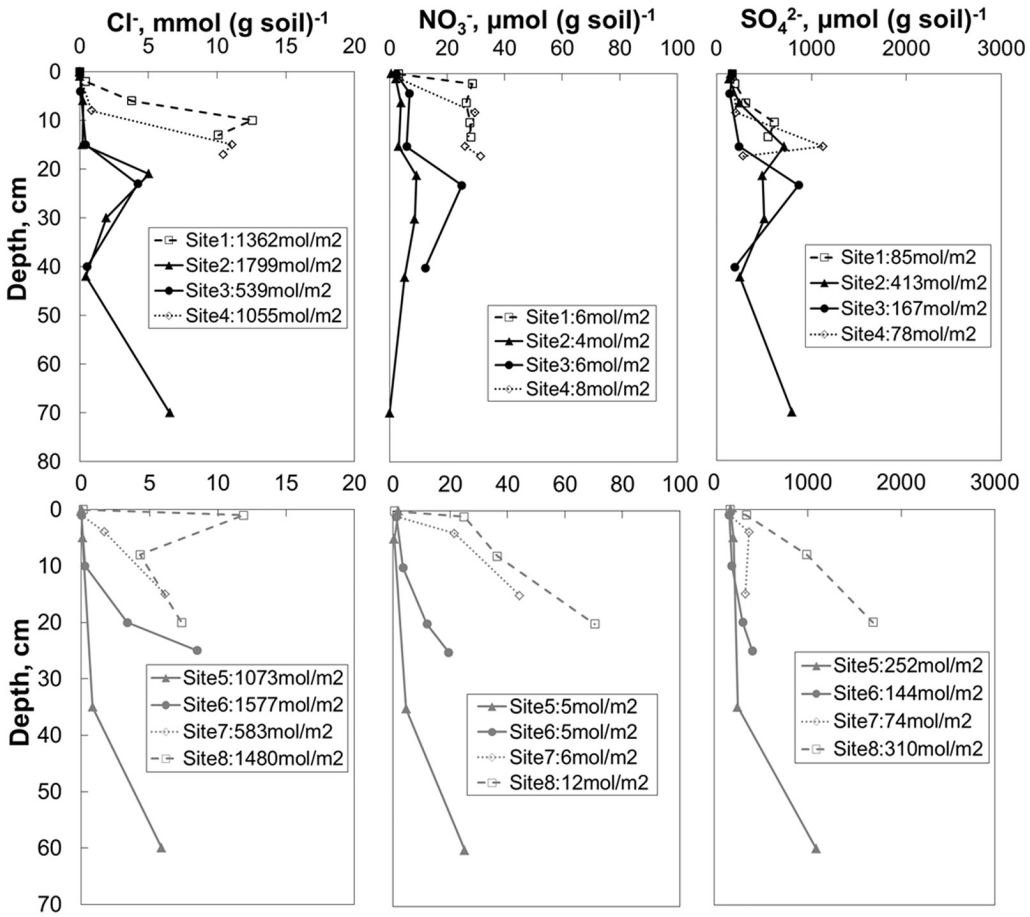

Fig. 6. The anion distribution as a function of depth for different sites along Transect 1 (upper panel) and Transect 2 (lower panel). Salt inventories are listed after the site number in the legend. Solid lines with solid-filled symbols in black or grey represent the BSC sites while dash lines with empty-filled symbols represent non-BSC sites. The surface samples at Sites 2, 3 and 5 are biological soil crust samples and their ion concentrations should be in the unit of mmol (g dry mass)$^{-1}$ or μmol (g dry mass)$^{-1}$.

(Muñoz-Schick et al., 2001), but they also resemble *Roccellina ochracea* shown in Follmann (2008). The genetic characterization of these BSCs is currently being investigated but a detailed phylogenic description is beyond the scope of this study.

5.2. The impact of BSCs on soil evolution

5.2.1. Soil profile depth

The significantly thicker soil profiles beneath BSCs could be attributed to the formation of hummocky grounds via possible geological processes that were not related to BSCs. Hummocky grounds could have formed when barren ground soils were partially eroded during an earlier epoch when there were large-scale surface drainage and

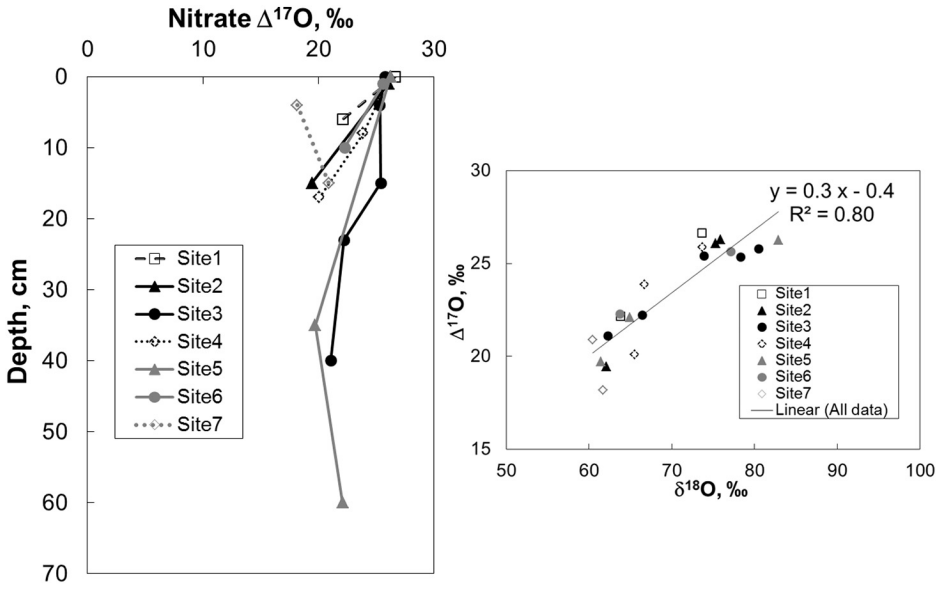

Fig. 7. Nitrate oxygen isotopic variations: $\Delta^{17}O$ depth profile (left); $\Delta^{17}O$ versus $\delta^{18}O$ (right). Solid-filled symbols in black or grey represent the BSC sites while empty-filled symbols represent non-BSC sites.

Table 2
A comparison of $^{36}Cl/Cl$ ratios at two sites, one with BSCs and one without BSCs. The first number of the sample ID indicates the site number while the second number after the dash delineates the sample order at each sampling site.

Sample ID	Depth, cm	$^{36}Cl/Cl$, $\times 10^{-15}$	^{36}Cl concentrations, $\times 10^6$ atoms $(g\ soil)^{-1}$
Site 1 on barren ground			
S1-1	Surface	398 ± 25	3.4
S1-2	0–4 cm	78 ± 5	19.2
S1-3	4–8 cm	125 ± 10	285.7
S1-4	8–12 cm	81 ± 5	612.1
S1-5	12–15 cm	97 ± 13	588.4
	^{36}Cl inventory, atoms m^{-2}		7.6×10^{13}
Site 2 on BSC-covered ground			
S2-3	2–10 cm	45 ± 3	6.7
S2-4	10–20 cm	37 ± 2	4.7
S2-5	20–22 cm	55 ± 6	166.6
S2-7	36–48 cm	78 ± 3	21.5
S2-8	70 cm	67 ± 3	264.3
	^{36}Cl inventory, atoms m^{-2}		1.2×10^{14}

frequent high winds in the Salar Grande region (Brüggen, 1950; Stoertz and Ericksen, 1974). The subsequent settlement of BSCs on hummocky grounds, rather than barren grounds, may have been the result of being isolated from the underlying salt layers that might have inhibited BSCs colonization.

Alternatively, the establishment of BSCs themselves could have impacted the soil evolution and also partly accounts for the development of thicker soil profiles beneath them. Because of limited biological and hydrological processes, the soil formation in hyper-arid Atacama has been suggested to be a simple long term accumulation of atmospheric deposition (Ewing et al., 2006; Wang, 2013). This mechanism of soil accumulation via the retention of atmospheric deposition has been supported by three major lines of evidence: (1) the Atacama salt deposits mainly originate from atmospheric photochemical compounds (e.g. Bao et al., 2000; Michalski et al., 2004); (2) dust trap collectors mimicking desert pavements placed in the Atacama have shown a net accumulation of dust, salts and cosmogenic nuclides ^{10}Be and ^{36}Cl (Wang, 2013; Wang et al., 2014, 2015); (3) at some locations, the soil matrix, including meteoric ^{10}Be atoms, has accumulated as layers over time via atmospheric deposition during the past ~6.6 My (Wang et al., 2015). The surfaces of BSC-covered grounds or barren grounds are all soft and the soil profiles consist of loosely-cemented sands and fragile aggregates, similar to those observed for the soil matrix by Wang et al. (2015), suggesting a similar soil accumulation mechanism at work in this study area. This soil accumulation could have been enhanced by the fractures and upturned edges of the BSCs that allow atmospheric or wind-blown dust and salts to migrate beneath them and protected the underlying material from subsequent wind erosion (Belnap, 2003; Belnap et al., 2014). Therefore, we hypothesized that the BSC coverage itself has promoted a significant soil accumulation over time and partly explains the thickness of the underlying soil profiles.

5.2.2. Grain size distribution

Two possible mechanisms may explain the greater amounts of fine particles beneath BSCs relative to beneath barren surfaces. The first is that BSCs may trap more fine particles in wind-blown or atmospheric dust and protect them from wind erosion. This is consistent with previous studies that BSCs enhanced the fine particle retention in the underlying soils (Li et al., 2005; Zhao et al., 2010). Alternatively, the BSCs may facilitate in situ weathering by breaking large particles into small particles due to soil amelioration (Schwartzman and Volk, 1989; Li et al., 2005). In view of the < 2 mm modern MAP (Houston, 2006) and the small number of foggy days at our site (~20 days per year) (Cereceda and Schemenauer, 1991) as well as the resistance of local rocks to breakdown, the production of fine particles via in situ weathering is likely very slow. The finest grain sizes were most abundant at depths of 10–15 cm at BSC sites or near the surface at non-BSC sites in Transect 1, suggesting the enhanced retention of fine particles in relatively modern times. Thus, we argue that the greater abundance of fine particles below BSCs is due to the greater retention of fine particles by BSCs themselves relative to barren soils.

5.3. The impact on salt geochemistry

The molar ratios of all soil ions indicated that the presence of gypsum ($CaSO_4{\cdot}2H_2O$) or anhydrite ($CaSO_4$) near the surface, while halite and other sulfate minerals such as thenardite (Na_2SO_4), darapskite ($Na_3(NO_3)(SO_4){\cdot}H_2O$) and humberstonite ($K_3Na_7Mg_2(SO_4)_6(NO_3)_2{\cdot}6H_2O$) occur at depths. This is probably due to that the ions segregate into discrete ionic zones by leaching according to their respective solubilities during periodic rainfall or fog events (Figs. 5 and 6). When comparing the BSC sites and non-BSC sites, however, there are significant statistical differences in the ion inventories and concentrations, suggesting that the salt geochemistry was somehow affected by the BSC coverage. The larger ion inventories beneath BSCs coupled with the deeper soil profiles are consistent with the observations of an increased retention of atmospheric dust and salts at other locations where soils are covered with BSCs (Reynolds et al., 2000).

While the larger ion inventories may partially be due to longer-term stable accumulation, BSCs may also alter soil ion distributions by either extracting or excreting biologically important ions (Evans and Lange, 2001; Bowker et al., 2006). Ions such as K^+, Mg^{2+}, Ca^{2+} and NO_3^- are important compounds required for metabolism and cellular function, and they would be expected to be depleted in soils beneath BSCs as the organisms extract these ions to maintain vitality. This seems to be consistent with the observed lower K^+, Mg^{2+}, Ca^{2+} and NO_3^- concentrations in the upper 10 cm soil layers compared to non-BSC soils at the same depths (Figs. 5 and 6). However, there is also a concurrent decrease in Na^+ and Cl^- concentrations, which are generally considered conservative tracers resistant to biologic alterations, particularly at such high concentrations. In addition, the amounts of soil ion losses beneath BSCs appear significantly greater than those expected by uptake on a mass (molar) basis. For example, the observed change in the Mg^{2+}/K^+ molar ratio in the upper 10 cm soil layers between BSC sites and non-BSC sites is typically > 10, but biological soil crust had Mg^{2+} and K^+ concentrations of 6.6 ± 1.2 and 2.3 ± 0.1 μmol $(g\ dry\ mass)^{-1}$ (averaged from the surface samples of Sites 2, 3 and 5) with the Mg^{2+}/K^+ molar ratio of ~3. This may be due to that more Mg^{2+} is present in the water-insoluble fractions of crusts relative to K^+, or while biologic uptake may slightly alter soil ion concentrations, it cannot adequately explain the low ion concentration observed beneath the BSCs.

The oxygen isotope composition of soil nitrate could further help constrain the importance of biological processes and the possible role that biology is playing in ion depletion beneath BSCs. Some BSCs are known to assimilate NO_3^- (Gaio-Oliveira et al., 2005), which should decrease soil NO_3^- amount beneath the BSCs, similar to that observed (Fig. 7). On the other hand, some BSCs are known to produce NO_3^- as a byproduct of nitrogen fixation (Gaio-Oliveira et al., 2005; Johnson et al., 2007). For the majority of material or processes on Earth, isotopic abundances vary approximately in proportion to the differences in the masses of isotopes, which is referred as mass-dependent isotopic fractionations due to both kinetic and equilibrium processes (Sharp, 2007). The mass-dependent isotope effect for oxygen can be approximately expressed in delta notation as $\delta^{17}O \sim 0.52 \cdot \delta^{18}O$, and the isotopic compositions of most terrestrial samples follow this relationship (see review in Thiemens, 2006). However, notable deviations from the mass-dependent fractionations, i.e. "anomalous" ^{17}O excesses (referred to as mass-independent fractionation, MIF), have been observed during the photochemistry of oxygen in nature and can be quantified by $\Delta^{17}O = \delta^{17}O - 0.52\ \delta^{18}O$ (Miller, 2002; Thiemens, 2006). For

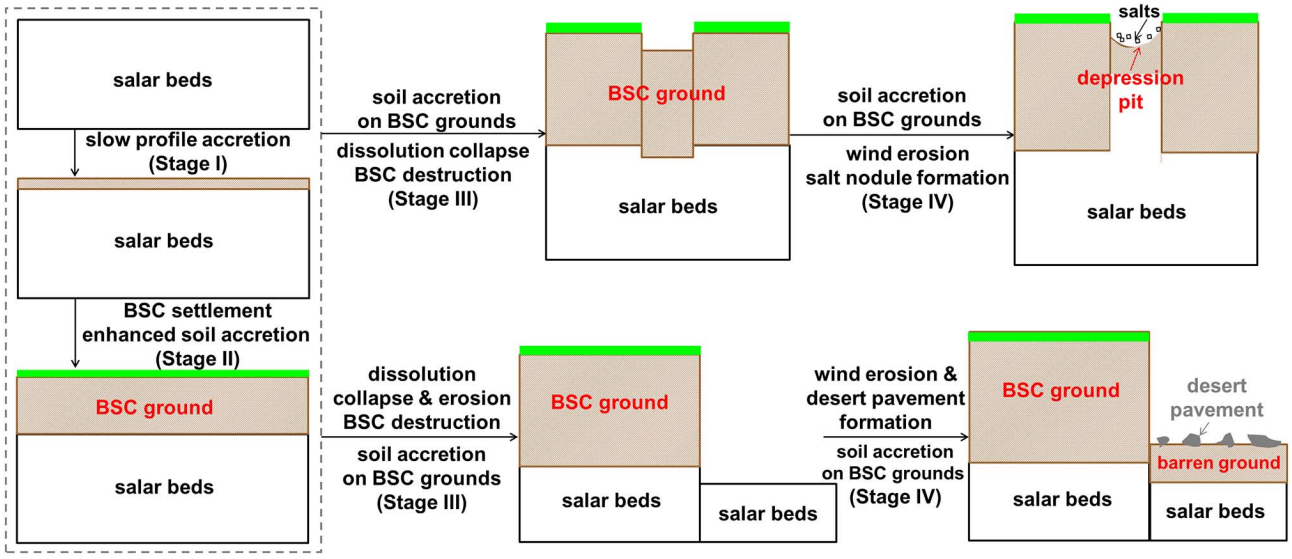

Fig. 8. Diagram of the proposed mechanism for soil evolution, including the development of the three major landscape features in the study area.

example, atmospheric nitrate has positive $\Delta^{17}O$ values of 20–35‰ (Michalski et al., 2003; Savarino et al., 2008) and its deposition to the surface results in $\Delta^{17}O$ anomalies in the Atacama nitrate minerals (Michalski et al., 2004). Soil nitrate $\Delta^{17}O$ values would provide another constraint on the relative role of deposition/erosion versus biologic alteration for causing the differences in soil ion concentration.

At both the BSC and non-BSC sites, all soil NO_3^- had large $\Delta^{17}O$ anomalies that also varied significantly with depths (Fig. 7). The surface nitrate $\Delta^{17}O$ values (26.1 ± 0.3‰, n = 7) are close to modern atmospheric nitrate $\Delta^{17}O$ of 25.8 ± 1.0‰ (n = 9) measured along a west-east transect across the Atacama (Wang et al., 2014), demonstrating that the surface soil nitrate is exclusively of atmospheric origin, not microbial nitrification (Michalski et al., 2004; Wang et al., 2016). The lower $\Delta^{17}O$ of soil nitrate at depths (18.2–25.3‰) could be explained by two mechanisms. The first is that soil NO_3^- deposits are comprised of a mixture of biotic NO_3^- ($\Delta^{17}O = 0$) and atmospheric NO_3^-. If preindustrial atmospheric NO_3^- had the same $\Delta^{17}O$ value as the modern dust trap NO_3^-, then matching the lowest soil NO_3^- $\Delta^{17}O$ value (18.2‰) would require nitrification rates to be (26.1–18.2)/26.1–30% of the preindustrial NO_3^- input rate. However, given the extremely low levels of water availability, a high level of nitrification should still be limited (Macduff and White, 1985). In addition, their nitrate concentrations are lower beneath the BSCs, not higher as would be expected for the addition of biologic nitrate. Instead, the soil NO_3^- $\Delta^{17}O$ values at two BSC sites (Sites 3 and 5) were generally higher than those at other sites, suggesting no additional inputs of NO_3^- by BSC nitrification. The second mechanism that could cause the changes in $\Delta^{17}O$ value with depth is a shift in the NO_x oxidation pathways that form NO_3^- as the atmospheric composition changed from an ancient unpolluted atmosphere to a modern polluted one. The lower soil nitrate $\Delta^{17}O$ at depths may reflect preindustrial atmospheric nitrate $\Delta^{17}O$ values that are a result of small local and global emissions of NO_x, as well as low levels of ozone, aerosols and biogenic gases in the troposphere (Alexander et al., 2009; Wang et al., 2014). The slope of 0.3 for soil nitrate $\Delta^{17}O$ and $\delta^{18}O$ (58.7–82.9‰) (Fig. 7) is close to that observed in atmospheric nitrate (0.8 for $\delta^{17}O$ vs. $\delta^{18}O$) (Michalski et al., 2004), further evidencing that the soil nitrate in this study is predominantly atmospheric nitrate. This suggests that this particular BSC species does not significantly nitrify, and since nitrate is readily available in Atacama soils, it could be used as a fixed nitrogen source for BSC metabolism, which is consistent with Gaio-Oliveira et al. (2005) who showed that lichens can directly take up NO_3^-. Therefore, the NO_3^- isotopic data do not support the hypothesis that BSCs are significantly altering the ion balance in soil beneath them, indicating that other processes are more important for controlling the ion distributions.

A second hypothesis for generally lower soil ion concentrations beneath BSCs is that BSCs aid in moisture retention with increased water infiltration that leads to enhanced downward leaching of salts. During rare rains or occasional fogs, if the water infiltration is enhanced, more salts would be leached from the upper layers to deeper sections, even lost to the salar beds. This seems in line with the observed low salt ion concentrations beneath BSCs. However, more leaching actually contradicts to the generally larger ion inventories at BSC sites compared to non-BSC sites. Also, Belnap (2006) suggested that BSCs might increase runoff and reduce water filtration in hyper-arid regions such as this study area. Therefore, the lower ion concentrations but larger ion inventories beneath BSCs could not be completely explained by leaching effects.

A third hypothesis to explain the generally lower ion concentrations at BSC sites (Figs. 5 and 6) is that the BSC sites are inclined to trap more dust relative to salts compared to the non-BSC sites. After deposition to barren soils, soluble salt ions or some of the very fine fractions of dust would tend to be transported downward by rare rains or occasional fogs. In contrast, most of the coarse dust particles would likely remain on the surface and lacking physical protection would subject them to wind erosion. The BSCs may provide physical protection needed to diminish erosion and enhance the retention of dust, which would simultaneously decrease the salt ion to dust ratios while increasing the total masses of accumulated materials. This would lead to larger ion inventories but smaller ion concentrations, which is consistent with our observations.

5.4. A proposed mechanism for soil evolution

To summarize, BSCs can limit erosion and enhance the retention of both dust and salts, likely to different extents, which subsequently impact the soil profile inflation and ion accumulation and distribution in this hyper-arid study area. Combining the current findings with those from past studies on surface processes in the Atacama, we propose a mechanism of soil accumulation via the retention of atmospheric deposition on the southeastern edge of the Salar Grande and the role of BSCs play in soil evolution. While the processes occur as a continuum, the mechanism is discussed as it relates to four stages of evolution (Fig. 8). During the first stage, atmospheric salts and dust deposit on barren salar beds to initiate soil development (Wang et al., 2016). In this early phase, the soil accretion should be very slow because of

significant wind erosion. During the second stage, the soil profile separates the surface from the salar beds, which would diminish the harmful effects of extremely saline environments to allow the settlement of BSCs on the surface (Amit et al., 2010). The fractures and upturned edges of the BSCs then facilitate more atmospheric deposition to infill below and inflate the profiles over time. During the third stage, wind activities may occur and directly erode away large surface areas, or subsurface groundwater may dissolve salts and transport them away from the salar edges causing the collapse of large surface areas (Brüggen, 1950). These two processes can both lead to destruction of BSCs and the formation of large concave barren grounds and relict hummocky grounds. Without the protection by BSCs, the new chaotic surface is likely attenuated and even completely eroded away by wind erosion. In the depression pits, the collection of salts from the pit edges and upward capillary flow may account for the formation of salt nodules on the pit surface (Stoertz and Ericksen, 1974). During the fourth stage, sparse desert pavements may begin to form on the barren grounds starting from rock material originating from the surrounding Coastal Range. Atmospheric salts, together with only trace amounts of moisture, can weather the rock material into small fragments (Cooke, 1981; Goudie et al., 2002). Atmospheric dust then fills in the voids and rock fractures to further advance the rock weathering; the sum of all this dust is the production of mineral gains as addition to the soil profile. The size of surface clasts or cobbles tend to become progressively smaller due to constant wind erosion, leading to the eventual development of a layer of clasts on the surface, i.e. desert pavement, and the surface becomes armored by a desert pavement (McFadden et al., 1987). While this soil accumulation process continues on the BSC-covered grounds, soil profile development may resume on barren grounds as well via the accumulation of atmospheric deposition with the protection of a desert pavement (McFadden et al., 1987; Anderson et al., 2002). Next we attempt to address the timescale of this soil accumulation.

5.5. The soil age constraints

The first estimate of the soil age was based on the soil accumulation mechanism and prior estimates of the local soil accumulation rate. A soil accumulation rate of 3.43×10^{-5} cm year^{-1} was previously derived from the meteoric ^{10}Be study at a soil pit site covered with a sparse desert pavement (Wang et al., 2015). Based on this rate, the ~15 cm deep soil profiles on barren grounds that were covered with a similarly sparse desert pavement would correspond to an accumulation age of 440 ky. The accumulation rate would not be applicable for estimating the ages of soil profiles beneath BSCs since the hypothesis is that the BSCs have altered the accumulation rate by stabilizing the surface and enhance material retention.

The age of the soil profiles can also be estimated using the ion inventory method. Assuming salts in the soil profile are all from the atmosphere and fully retained, the soil ion inventories should only relate to atmospheric salt deposition rates and the accumulation timescales. Na^+ and Cl^- inventories were deemed inappropriate for use as age constraints because the study area is on the rim of the halite-type Salar Grande basin and local NaCl deposition rates to the soils are likely significant (Stoertz and Ericksen, 1974). Soil ages based on other mineral ion inventories, such as K^+ and NO_3^-, would also likely underestimate the age of the insoluble material because they are easily mobile and could be quickly transported downward during a significant rainfall event. Thus, the Ca^{2+} and SO_4^{2-} inventories were used to estimate the soil ages. Atmospheric salt deposition rates measured using passive dust traps averaged for two sites ~200 km to the south of Salar Grande are 3.8 Ca^{2+} mmol m^{-2} year^{-1} and 6.6 SO_4^{2-} mmol m^{-2} year^{-1} (Table 2 in Wang et al., 2014), respectively. These deposition rates give the ages of 14–53 ky based on Ca^{2+} inventories and 13–63 ky based on SO_4^{2-} inventories. Because the salt inventory method is based on the assumption of no erosion or leaching losses that is almost unlikely, the most ancient age of 63 ky can still be considered as the minimum age constraint of the study area.

Though chloride is subject to substantial inputs of stable chloride from the Pacific Ocean and Salar Grande, radioactive ^{36}Cl might be used to constrain soil ages using the ^{36}Cl inventories. ^{36}Cl is mainly produced by spallation of argon by secondary cosmic rays in the atmosphere (Lal et al., 1958), while the in situ ^{36}Cl production via the spallation of Ca and K and thermal neutron absorption is typically one to two orders of magnitude slower (Bentley et al., 1986 and references therein). There should be no detectable ^{36}Cl in the Pliocene chloride that makes up the Salar Grande (Díaz et al., 1999) in view of this long residence of chloride and the ^{36}Cl radioactive property (half-life: 301 ky). The ocean is also known to contain massive stable chloride but limited cosmogenic ^{36}Cl with seawater ^{36}Cl/Cl ratio of $0.5 \pm 0.3 \times 10^{-15}$ (Argento et al., 2010). Therefore, the measureable ^{36}Cl in the soil should be neither from the Salar Grande nor the Pacific Ocean, but mainly from long-range transport and deposition of atmospheric compounds. The ^{36}Cl inventory is a balance between deposition and decay loss as a function of deposition rate, decay rate, and time. Assuming a constant meteoric ^{36}Cl flux and the full retention of ^{36}Cl, $I_{36Cl} = F_{36Cl} \cdot (1 - e^{-\lambda t}) / \lambda$, where I_{36Cl} is the ^{36}Cl inventory, F_{36Cl} is the meteoric ^{36}Cl flux, λ is the ^{36}Cl decay constant (2.25×10^{-6} year^{-1}), and t is the soil ^{36}Cl residence time. 10% of the estimated ^{36}Cl flux before the 1950s for the Huascarán ice core (1760 km to the northwest of our site) (Heikkilä et al., 2009), i.e. 2.2×10^8 atoms m^{-2} year^{-1}, was assumed as the meteoric ^{36}Cl deposition rate for this study area based on our previous ^{10}Be study (Wang et al., 2015). However, the ^{36}Cl inventories of 1.2×10^{14} atoms m^{-2} at Site 2 (Table 2) could not resolve a soil age, suggesting a ^{36}Cl legacy, i.e. $I_{36Cl} \neq 0$ when $t = 0$. The ^{36}Cl inventories of 7.6×10^{13} atoms m^{-2} at Site 1 (Table 2), instead, yielded the ^{36}Cl accumulation timescale of ~670 ky. Despite the match with the accumulation age of 440 ky, this ^{36}Cl accumulation timescale, however, may still have a significant amount of uncertainties due to rough estimates of the ^{36}Cl inventory and meteoric ^{36}Cl deposition rate, and more importantly, possible existence of ^{36}Cl legacies before the initiation of soil profile development and from sources other than in situ atmospheric deposition.

The highest ^{36}Cl/Cl ratio of 398×10^{-15} occurring on the surface of Site 1 (Table 2) is significantly higher than the surface ^{36}Cl/Cl ratios of 324×10^{-15} and 341×10^{-15} measured for a soil pit ~200 km to the southeast of this study area (Wang, 2013). Instead, the ^{36}Cl/Cl ratios beneath the surface were consistently low ($78–125 \times 10^{-15}$ at Site 1 and $37–78 \times 10^{-15}$ at Site 2) (Table 2), indicating that large chloride inputs from the Pacific Ocean and the halite-type Salar Grande suppressed the ^{36}Cl/Cl ratios, and significant water events or capillary migration of ground water in ancient times likely homogenized the ^{36}Cl/Cl ratios in each profile. The mostly likely explanation for the high surface ^{36}Cl/Cl ratio of 398×10^{-15} is that it represents deposition of nuclear bomb produced ^{36}Cl in the 1950s, i.e. a ^{36}Cl bomb spike (Phillips et al., 1986), which was also observed in the Huascarán ice core (Heikkilä et al., 2009). This suggests that occasional fogs or rains have been unable to move salts to lower depths of soil profiles in the last 60 years, which might be due to faster upward evaporation relative to downward water infiltration.

6. Conclusions

BSCs have the potential to protect the soil beneath from wind erosion and enhance soil accretion by trapping more atmospheric dust and salts. The enhanced retention of atmospheric dust, especially fine particles, may partially explain the thicker loose soil profiles and higher fine particle fractions beneath BSCs than at non-BSC sites. The generally larger salt ion inventories and smaller salt ion concentrations at BSC sites can further be due to the enhanced retention of dust relative to salts, thus decreasing the salt ion to dust ratios but increasing the total accumulated ion masses. Nitrate oxygen isotope data indicated that

BSCs can probably directly use soil nitrates originated from atmospheric deposition rather than nitrify, pointing out that biological processes of BSCs may not significantly impact the salt geochemistry in the underlying soils.

A mechanism of consistent soil accumulation via the retention of atmospheric deposition and occasional interruption of subsurface collapsing due to erosion processes was proposed to explain the development of soil profiles and different landscape features as well as the role of BSCs in soil evolution in this study area. Soil profiles ages were further constrained to be around 440 ky using soil profile depths based on the soil accumulation mechanism, while the ion (including ^{36}Cl) inventory methods were subject to large uncertainties for age estimates. A bomb spike with the $^{36}Cl/Cl$ ratio of 398×10^{-15} was preserved on the surface at a non-BSC site likely over the past 60 years, suggesting the extraordinary stability of the surface, corresponding to the unique soil evolution and salt geochemistry in this hyper-arid study area.

Acknowledgements

This work was supported by the United States National Science Foundation Grants to GM (EAR 0922114) and to MC (EAR 1153689), the Geological Society of America Graduate Student Research Grant to FW, and several fellowships from Purdue University to FW (Purdue Climate Change Research Center fellowship, Purdue Research Foundation research assistantship and Purdue Bilsland Dissertation fellowship) as well as the postdoctoral funding from Peking University Shenzhen Graduate School. We thank Nathaniel Louden, Brenda Bowen, Susan Ma, Raul Ochoa, and Ji-Hye Seo for assistance in the lab and field.

References

Alexander, B., Hastings, M., Allman, D., Dachs, J., Thornton, J., Kunasek, S., 2009. Quantifying atmospheric nitrate formation pathways based on a global model of the oxygen isotopic composition ($\Delta^{17}O$) of atmospheric nitrate. Atmos. Chem. Phys. 9, 5043–5056.

Amit, R., Enzel, Y., Grodek, T., Crouvi, O., Porat, N., Ayalon, A., 2010. The role of rare rainstorms in the formation of calcic soil horizons on alluvial surfaces in extreme deserts. Quat. Res. 74, 177–187.

Anderson, K., Wells, S., Graham, R., 2002. Pedogenesis of vesicular horizons, Cima volcanic field, Mojave Desert, California. Soil Sci. Soc. Am. J. 66, 878–887.

Argento, D.C., Stone, J.O., Fifield, L.K., Tims, S.G., 2010. Chlorine-36 in seawater. Nucl. Instrum. Methods Phys. Res. 268 (7–8), 1226–1228.

Bao, H., Thiemens, M.H., Farquhar, J., Campbell, D.A., Lee, C.C.W., Heine, K., Loope, D.B., 2000. Anomalous ^{17}O compositions in massive sulphate deposits on the Earth. Nature 406, 176–178.

Belnap, J., 2002. Nitrogen fixation in biological soil crusts from southeast Utah, USA. Biol. Fertil. Soils 35 (2), 128–135.

Belnap, J., 2003. The world at your feet: desert biological soil crusts. Front. Ecol. Environ. 1, 181–189.

Belnap, J., 2006. The potential roles of biological soil crusts in dryland hydrologic cycles. Hydrol. Process. 20, 3159–3178.

Belnap, J., Gardner, J.S., 1993. Soil microstructure in soils of the Colorado Plateau: the role of the cyanobacterium *Microcoleus vaginatus*. West. N. Am. Nat. 53, 40–47.

Belnap, J., Phillips, S.L., Miller, M.E., 2004. Response of desert biological soil crusts to alterations in precipitation frequency. Oecologia 141 (2), 306–316.

Belnap, J., Walker, B.J., Munson, S.M., Gill, R.A., 2014. Controls on sediment production in two US deserts. Aeolian Res. 14, 15–24.

Bentley, H.W., Phillips, F.M., Davis, S.N., 1986. Chlorine-36 in the terrestrial environment. In: Fritz, P., Fontes, J.C. (Eds.), Handbook of Environmental Isotope Geochemistry. Elsevier, Amsterdam.

Bowker, M.A., Belnap, J., Davidson, D.W., Goldstein, H.L., 2006. Correlates of biological soil crust abundance across a continuum of spatial scales: support for a hierarchical conceptual model. J. Appl. Ecol. 43 (1), 152–163.

Brüggen, J., 1950. Fundamentos de Ia geologia de Chile. Instituto Geográfico Militar, Santiago, Chile.

Büdel, B., 2001. Biological soil crusts of South America. In: Belnap, J., Lange, O.L. (Eds.), Biological Soil Crusts: Structure, Function, and Management. Springer, Berlin, pp. 51–55.

Cereceda, P., Schemenauer, R.S., 1991. The occurrence of fog in Chile. J. Appl. Meteorol. Climatol. 30, 1097–1105.

Conley, C.A., Ishkhanova, G., McKay, C.P., Cullings, K., 2006. A preliminary survey of non-lichenized fungi cultured from the hyperarid Atacama Desert of Chile. Astrobiology 6, 521–526.

Cooke, R.U., 1970. Stone pavements in deserts. Ann. Assoc. Am. Geogr. 60, 560–577.

Cooke, R.U., 1981. Salt weathering in deserts. Proc. Geol. Assoc. 92, 1–16.

Craig, H., 1961. Standard for reporting concentrations of deuterium and oxygen-18 in natural waters. Science 133, 1833–1834.

Díaz, G.C., Mendoza, M., García-Veigas, J., Pueyo, J.J., Turner, P., 1999. Evolution and geochemical signatures in a Neogene forearc evaporitic basin: the Salar Grande (Central Andes of Chile). Palaeogeogr. Palaeoclimatol. Palaeoecol. 151, 39–54.

Ericksen, G.E., 1981. Geology and origin of the Chilean nitrate deposits. In: U.S. Geological Survey Professional Paper 1188, pp. 37.

Evans, R.D., Lange, O.L., 2001. Biological soil crusts and ecosystem nitrogen and carbon dynamics. In: Lange, O.L. (Ed.), Biological Soil Crusts: Structure, Function and Management. Springer-Verlag, Berlin, pp. 263–279.

Ewing, S.A., Sutter, B., Owen, J., Nishiizumi, K., Sharp, W., Cliff, S.S., Perry, K., Dietrich, W., McKay, C.P., Amundsona, R., 2006. A threshold in soil formation at Earth's arid–hyperarid transition. Geochim. Cosmochim. Acta 70, 5293–5322.

Flores-Aqueveque, V., Alfaro, S.C., Caquineau, S., Foret, G., Vargas, G., Rutllant, J.A., 2012. Inter-annual variability of southerly winds in a coastal area of the Atacama Desert: implications for the export of aeolian sediments to the adjacent marine environment. Sedimentology 59 (3), 990–1000.

Follmann, G., 2008. Two new crustaceous soil lichens (Arthoniales) from the Chilean Atacama Desert, South America. Herz 21, 2–39.

Gaio-Oliveira, G., Dahlman, L., Palmqvist, K., Martins-Loucao, M.A., Máguas, C., 2005. Nitrogen uptake in relation to excess supplyand its effects on the lichens *Evernia prunastri* (L.) Ach and *Xanthoria parietina* (L.) Th. Fr. Planta 220, 794–803.

Goudie, A.S., Wright, E., Viles, H.A., 2002. The roles of salt (sodium nitrate) and fog in weathering: a laboratory simulation of conditions in the northern Atacama Desert, Chile. Catena 48, 255–266.

Hainsworth, L.J., Mignerey, A.C., Helz, G.R., Sharma, P., Kubik, P.W., 1994. Modern chlorine-36 deposition in southern Maryland, USA. Nucl. Inst. Methods Phys. Res. B 92, 345–349.

Heikkilä, U., Beer, J., Feichter, J., Alfimov, V., Synal, H., Schotterer, U., Eichler, A., Schwikowski, M., Thompson, L., 2009. ^{36}Cl bomb peak: comparison of modeled and measured data. Atmos. Chem. Phys. 9, 4145–4156.

Housman, D.C., Powers, H.H., Collins, A.D., Belnap, J., 2006. Carbon and nitrogen fixation differ between successional stages of biological soil crusts in the Colorado Plateau and Chihuahuan Desert. J. Arid Environ. 66 (4), 620–634.

Houston, J., 2006. Variability of precipitation in the Atacama Desert: its causes and hydrological impact. Int. J. Climatol. 26, 2181–2198.

Johnson, S.L., Neuer, S., Garcia-Pichel, F., 2007. Export of nitrogenous compounds due to incomplete cycling within biological soil crusts of arid lands. Environ. Microbiol. 9, 680–689.

Kaiser, J., Hastings, M.G., Houlton, B.Z., Röckmann, T., Sigman, D.M., 2007. Triple oxygen isotope analysis of nitrate using the denitrifier method and thermal decomposition of N_2O. Anal. Chem. 79, 599–607.

Krumbein, W.C., Sloss, L.L., 1963. Stratigraphy and Sedimentation, 2nd edition. W.H. Freeman & Co., San Francisco, CA, USA.

Lal, D., Malhotra, P., Peters, B., 1958. On the production of radioisotopes in the atmosphere by cosmic radiation and their application to meteorology. J. Atmos. Terr. Phys. 12, 306–328.

Leys, J.F., Eldridge, D.J., 1998. Influence of cryptogamic crust disturbance to wind erosion on sand and loam rangeland soils. Earth Surf. Process. Landf. 23, 963–974.

Li, W.H., Ren, T.R., Zhou, Z.B., 2005. Study on the soil physicochemical characteristics of biological crust on sand dune surface in Gurbantünggtüt Desert, Xinjiang Region. J. Glaciol. Geocryol. 27, 619–627.

Macduff, J.H., White, R.E., 1985. Net mineralization and nitrification rates in a clay soil measured and predicted in permanent grassland from soil temperature and moisture content. Plant Soil 86 (2), 151–172.

McFadden, L.D., Wells, S.G., Jercinovich, M.J., 1987. Influences of eolian and pedogenic processes on the origin and evolution of desert pavements. Geology 15, 504–508.

McKay, C.P., Friedmann, E.I., Gómez-Silva, B., Cáceres-Villanueva, L., Andersen, D.T., Landheim, R., 2003. Temperature and moisture conditions for life in the extreme arid region of the Atacama Desert: four years of observations including the El Niño of 1997–1998. Astrobiology 3, 393–406.

Michalski, G., Scott, Z., Kabiling, M., Thiemens, M., 2003. First measurements and modeling of ^{17}O in atmospheric nitrate. Geophys. Res. Lett. 30, 1870.

Michalski, G., Böhlke, J.K., Thiemens, M., 2004. Long term atmospheric deposition as the source of nitrate and other salts in the Atacama Desert, Chile: new evidence from mass-independent oxygen isotopic compositions. Geochim. Cosmochim. Acta 68, 4023–4038.

Miller, M., 2002. Isotopic fractionation and the quantification of ^{17}O anomalies in the oxygen three-isotope system: an appraisal and geochemical significance. Geochim. Cosmochim. Acta 66, 1881–1889.

Muñoz-Schick, M., Pinto, R., Mesa, A., Moreira-Muñoz, A., 2001. Fog oases during the El Niño Southern Oscillation 1997–1998, in the coastal hills south of Iquique, Tarapacá region, Chile. Rev. Chil. Hist. Nat. 74 (2), 389–405.

Phillips, F.M., Bentley, H.W., Davis, S.N., Elmore, D., Swanick, G.B., 1986. Chlorine 36 dating of very old groundwater: 2. Milk River aquifer, Alberta, Canada. Water Resour. Res. 22, 2003–2016.

Placzek, C., Matmon, A., Granger, D., Quade, J., Niedermann, S., 2010. Evidence for active landscape evolution in the hyperarid Atacama from multiple terrestrial cosmogenic nuclides. Earth Planet. Sci. Lett. 295, 12–20.

Reynolds, J.F., Kemp, P.R., Tenhunen, J.D., 2000. Effects of long-term rainfall variability on evapotranspiration and soil water distribution in the Chihuahuan Desert: a modeling analysis. Plant Ecol. 150, 145–159.

Riha, K.M., 2013. The Use of Stable Isotopes to Constrain the Nitrogen Cycle. Purdue University (PhD dissertation).

Rundel, P.W., 1978. Ecological relationships of desert fog zone lichens. Bryologist 81, 277–293.

Savarino, J., Bhattacharya, S., Morin, S., Baroni, M., Doussin, J.F., 2008. The NO + O reaction: a triple oxygen isotope perspective on the reaction dynamics and atmospheric implications for the transfer of the ozone isotope anomaly. J. Chem. Phys. 128, 194303.
Schwartzman, D.W., Volk, T., 1989. Biotic enhancement of weathering and the habitability of Earth. Nature 340, 457–460.
Sharma, P., Bourgeois, M., Elmore, D., Granger, D., Lipschutz, M.E., Ma, X., Miller, T., Mueller, K., Rickey, F., Simms, P., Vogt, S., 2000. PRIME lab AMS performance, upgrades and research applications. Nucl. Instrum. Methods Phys. Res. 172, 112–123.
Sharp, Z., 2007. Principles of Stable Isotope Geochemistry. Pearson Education, Upper Saddle River, USA.
Stivaletta, N., Barbieri, R., Billi, D., 2012. Microbial colonization of the salt deposits in the driest place of the Atacama Desert (Chile). Orig. Life Evol. Biosph. 42, 187–200.
Stoertz, G.E., Ericksen, G.E., 1974. Geology of salars in northern Chile. In: US Geological Survey Professional Paper, pp. 811.
Tehler, A., 1983. The Genera Dirina and Roccellina (Roccellaceae). Nord. J. Bot. 3 (5), 628.
Thiemens, M.H., 2006. History and applications of mass-independent isotope effects. Annu. Rev. Earth Planet. Sci. 34, 217–262.
Wang, F., 2013. The Mechanism and Timescales of Soil Formation in the Hyper-arid Atacama Desert, Chile. Purdue University (PhD thesis).
Wang, F., Michalski, G., Seo, J.H., Ge, W.S., 2014. Geochemical, isotopic, and mineralogical constraints on atmospheric deposition in the hyper-arid Atacama Desert, Chile. Geochim. Cosmochim. Acta 135, 29–48.
Wang, F., Michalski, G., Seo, J.H., Granger, D.E., Caffee, M., 2015. Beryllium-10 concentrations in the hyper-arid soils in the Atacama Desert, Chile: implications for arid soil formation rates and El Niño driven changes in Pliocene precipitation. Geochim. Cosmochim. Acta 160, 227–242.
Wang, F., Ge, W.S., Luo, H., Seo, J.H., Michalski, G., 2016. Oxygen-17 anomaly in soil nitrate: a new precipitation proxy for desert landscapes. Earth Planet. Sci. Lett. 438, 103–111.
Zhao, H.L., Guo, Y.R., Zhou, R.L., Drake, S., 2010. Biological soil crust and surface soil properties in different vegetation types of Horqin Sand Land, China. Catena 82, 70–76.